CONF-840807--3

CHEMICAL THERMODYNAMIC REPRESENTATION OF $\langle UO_{2\pm x} \rangle$*

Terrence B. Lindemer and Theodore M. Besmann
Chemical Technology Division
Oak Ridge National Laboratory
Oak Ridge, Tennessee 37831
USA

CONF-840807--3

DE84 016666

To be presented at the IUPAC Conference on Chemical Thermodynamics, August 13–17, 1984, McMaster University, Hamilton, Canada

*Research sponsored by the Division of Materials Sciences, U.S. Department of Energy under contract DC-AC05-840R21400 with the Martin Marietta Energy Systems, Inc.

CHEMICAL THERMODYNAMIC REPRESENTATION OF $\langle UO_{2\pm x} \rangle$*

Terrence B. LINDEMER and Theodore M. BESMANN
Chemical Technology Division, Oak Ridge National Laboratory, Oak Ridge, Tennessee 37831

The entire $\langle UO_{2\pm x} \rangle$** data base for the dependence of the nonstoichiometry, x, on temperature and chemical potential of oxygen (oxygen potential) was retrieved from the literature and represented. This data base was interpreted by least-squares analysis using equations derived from the classical thermodynamic theory for the solid solution of a solute in a solvent. For hyperstoichiometric oxide at oxygen potentials more positive than -266700 + 16.5T kJ/mol, the data were best represented by a $[UO_2]$-$[U_3O_7]$ solution. For O/U ratios above 2 and oxygen potentials below this boundary, a $[UO_2]$-$[U_2O_{4.5}]$ solution represented the data. The $\langle UO_{2-x} \rangle$ data were represented by a $[UO_2]$-$[U_{1/3}]$ solution. The resulting equations represent the experimental $\ln(p^*_{O_2})$-$\ln(x)$ behavior and can be used in thermodynamic calculations to predict phase boundary compositions consistent with the literature. Collectively, the present analysis permits, for the first time, a mathematical representation of the behavior of the total data base.

1. INTRODUCTION

The use of actinide oxides as nuclear fuels has led to a very large data base on the nonstoichiometry of uranium dioxide, plutonium dioxide, rare-earth dioxides, and their mutual solid solutions. The portion of the data base of interest here consists of the T-x-$p^*_{O_2}$ interdependence, where T is the temperature in kelvin, x the deviation from stoichiometry, and

---

*Research sponsored by the Division of Materials Sciences, U.S. Department of Energy under contract DC-AC05-84OR21400 with the Martin Marietta Energy Systems, Inc.

**The symbols < >, [ ], { }, and ( ) denote crystalline solid, solid-solution species, liquid, and gas respectively.

$p^*_{O_2}$ the pressure of oxygen in units of MPa divided by the standard-state oxygen pressure, 0.101 MPa. This paper and a companion paper are the first two of a series in which these data are represented by the chemical thermodynamics of the mutual solid solution of elements or compounds. It appears that only Hoch and coworkers[1,2] have applied this methodology to the actinide oxide systems.

The representation used here presumes that the chemical activities of the actinide and oxygen in the fluorite-structure phases can be described by a solution of two species. The solvent species is chosen to have the stoichiometry of the undefected phase, in this case $[UO_2]$, and the solute species is chosen to reflect, together with the solvent, the oxygen potential-temperature-composition behavior and the system phase relations. This allows use of the species in reactions to describe phase boundaries and chemical potentials in an easy and convenient manner. It is realized, however, that combinations of the species to form defected fluorite crystal lattices may not be possible. Further, the configurational entropy resulting from the assumption that the species are randomly mixed is not accurate because of the impossibility of predicting allowed lattice site positions.

2. DATA BASE

The relevant data base for nonstoichiometric urania is summarized in table 1 and fig. 1. Collectively, ~1780 x-T-$p^*_{O_2}$ values have been reported. All these data have been compiled in one Oak Ridge National Laboratory document, along with similar data for the U-Pu-O system.[40] Since many of the original data were given

graphically, a brief explanation of the digitization of these data is in order. Each figure from the original references was photocopied, and small figures were then enlarged. The copy was taped to graph paper with the coordinate axes of the figure coincident with those of the graph paper, and a pin was used to punch a hole through the data points and the graph paper. The coordinate values were read from the graph paper in mm and converted by a computer program to values of T, O/U, and the chemical potential of oxygen [RT ln ($p^*_{O_2}$), with R being the ideal gas constant]. In addition, the program calculated the values of the data in the units given on the original figure. These values were then compared with the figure so that, as far as could be determined, any errors in data extraction and conversion were eliminated.

3. BASIS OF THE REPRESENTATION

The nonstoichiometry of uranium dioxide will be represented by a solution of two fluorite-structure, face-centered-cubic (fcc) species having different O/U ratios. One species will be [UO_2] and the other [U_aO_b]. The moles, m, of each species in the solution are calculated from the mass-balance equations for uranium and oxygen, respectively,

$$1 = m_{UO_2} + a\, m_{U_aO_b} , \qquad (1)$$

and

$$O/U = 2 \pm x = 2\, m_{UO_2} + b\, m_{U_aO_b} . \qquad (2)$$

The standard Gibbs free energy of the solution is defined as

$$\Delta G_f^o\langle UO_{2\pm x}\rangle = n_{UO_2}\ \Delta G_f^o\langle UO_2\rangle + n_{U_aO_b}\Delta G_f^o\langle U_aO_b\rangle_{fcc} + n_{UO_2}\ RT\ \ln\ (n_{UO_2}) + n_{U_aO_b}\ RT\ \ln\ (n_{U_aO_b}) + E\ n_{UO_2}n_{U_aO_b}\ , \quad (3)$$

in which E is the energy of interaction between the solid-solution species, n_i denotes the mole fraction of species i, and $\Delta G_f^o\langle i\rangle$ is the standard Gibbs free energy of formation of species i from the elements in their standard states. Note that the standard states of both species in the solution are defined here as having the fcc, fluorite structure. The partial molal free energy expressions are very useful because they can be used directly in equilibrium calculations. These are obtained for species i by the operation

$$\frac{\partial[(m_1 + m_2)\ \Delta G_f^o\langle UO_{2\pm x}\rangle]}{\partial m_i} = \Delta\bar{G}[i]\ . \quad (4)$$

This leads to

$$\Delta\bar{G}[UO_2] = \Delta G_f^o\langle UO_2\rangle + RT\ \ln\ (n_{UO_2}) + E\ n^2_{U_aO_b} \quad (5)$$

and

$$\Delta\bar{G}[U_aO_b] = \Delta G_f^o\langle U_aO_b\rangle_{fcc} + RT\ \ln\ (n_{U_aO_b}) + E\ n^2_{UO_2} \quad (6)$$

4. ANALYSIS OF DATA

About 130 T-x-$p^*_{O_2}$ values were removed from the data base during the course of the analysis. As will be demonstrated later, these 130 values appeared to be inconsistent with the behavior of the rest. The rejected sets were those of Chapman and Meadows,[12] Chilton and Kirkham,[32] Tetenbaum and Hunt's $\langle UO_{2+x}\rangle$ data,[20] and Swanson.[31] See section 5 for further discussion

of Tetenbaum and Hunt's data. None of these data were used in the least-squares analyses, although they are plotted in several of the figures to show their deviation from the rest. Least-squares analysis of the accepted data was always performed with equal weighting of the T-x-$\ln(p^*_{O_2})$ values.

4.1 $\langle UO_{2+x} \rangle$, high hyperstoichiometry

It is generally recognized that isothermal x-$p^*_{O_2}$ data plotted as ln(x) vs $\ln(p^*_{O_2})$ shows a change in slope at about O/U = 2.01. Examination of all the raw data exhibiting this transition revealed that this change can be better defined as occurring at a constant oxygen potential of about -260 kJ/mol. The data more positive than this oxygen potential value will be analyzed first.

A least-squares analysis of this portion of the data base was made utilizing the equation

$$\ln (p^*_{O_2}) = a/T + b + c \ln(x) . \qquad (7)$$

The slope, c, was 2.21 for the range $2.01 < O/U < 2.1$. This is within 10% of the commonly reported slope of 2. Above O/U = 2.1, the slope increases continuously. Both of these features are shown in fig. 2 for a typical data set obtained by combining Hagemark and Broli's data,[16] for which T = 1673 K and $2.094 < O/U < 2.239$, with Roberts and Walter's data,[5] for which T = 1675 K and $2.01 < O/U < 2.225$. It is the behavior of the region above O/U = 2.1 that permitted the choice of the proper solute species.

The procedure for deducing which solute oxide should be used in solution with $[UO_2]$ commenced by considering the several different equilibria to be given below. The solvent oxide is always $[UO_2]$, and the solute oxides are known

oxides of uranium except for $[U_2O_5]$, which was included because it represents the hypothetical oxide formed from U^{+5}, and $[U_{10/3}O_{23/3}]$ (O/U = 2.3), which can be considered to be slightly substoichiometric $[U_3O_7]$ (O/U = 2.33). The T-x-ln $(p^*_{O_2})$ relationship corresponding to each equilibrium is also given below assuming E = 0. For the equilibrium $2[UO_2] + (O_2) \leftrightharpoons 2[UO_3]$,

$$RT \ln (p^*_{O_2}) = \Delta H^o_{rxn} - T\Delta S^o_{rxn} + 2\,RT \ln (x/(1-x)) \quad . \tag{8}$$

in which ΔH_{rxn} and ΔS_{rxn} are the usual product-reactant differences in enthalpy of formation and entropy, respectively, for a particular equilibrium. For the equilibrium $4[UO_2] + (O_2) \leftrightharpoons 2[U_2O_5]$,

$$RT \ln (p^*_{O_2}) = \Delta H^o_{rxn} - T\Delta S^o_{rxn} + 2\,RT \ln \frac{x(1-x)}{(1-2x)^2} \quad . \tag{9}$$

For the equilibrium $6[UO_2] + (O_2) \leftrightharpoons 2[U_3O_7]$,

$$RT \ln (p^*_{O_2}) = \Delta H^o_{rxn} - T\Delta S^o_{rxn} + 2\,RT \ln \frac{x(1-2x)^2}{(1-3x)^3} \quad . \tag{10}$$

For the equilibrium $(20/3)[UO_2] + (O_2) \leftrightharpoons 2[U_{10/3}O_{23/3}]$,

$$RT \ln (p^*_{O_2}) = \Delta H^o_{rxn} - T\Delta S^o_{rxn} + 2\,RT \ln \frac{x(1-2.33x)^{2.33}}{(1-3.33x)^{3.33}} \quad . \tag{11}$$

For the equilibrium $8[UO_2] + (O_2) \leftrightharpoons 2[U_4O_9]$,

$$RT \ln (p^*_{O_2}) = \Delta H^o_{rxn} - T\Delta S^o_{rxn} + 2\,RT \ln \frac{x(1-3x)^3}{(1-4x)^4} \quad . \tag{12}$$

At this stage of the analysis, one is concerned with finding which one of the several equations will actually result in a slope of 2 over the entire range of x. Therefore, for the data set given in fig. 2, it is sufficient to divide each of the above equations by RT and to plot $\ln(p^*_{O_2})$ versus each of the several $\ln(f(x))$ terms. Figure 2 illustrates the resulting plots. Coincidence of any one plot of $\ln(f(x))$ with the line having a slope of two would indicate that that particular function, and thus a particular solid solution, was most representative of the data.

Several observations can be made from fig. 2. It is clear that the representations based on the solutes $[U_3O_7]$ or $[U_{10/3}O_{23/3}]$ come closest to giving a slope of two over the entire range of x. (In fact, the observation that the $[UO_2]$-$[U_3O_7]$ solution did not quite give the desired relationship for this particular data subset led to the use of the $U_{10/3}O_{23/3}$ composition.) It can also be seen that all the representations give a slope close to 2 at the smaller values of x, or, more specifically, at $x < 0.05$. It follows that very nonstoichiometric data are necessary in order to permit the general application of the present methods to other nonstoichiometric systems. Finally, the present technique provides a sensitive indication of the O/U ratio of the solute oxide; ratios of 2.3 to 2.33 appear close to those needed, while ratios of 2.5 (from $[U_2O_5]$) or 2.25 (from $[U_4O_9]$) are wide of the mark. It can also be seen from the equation for the $[UO_2]$-$[U_4O_9]$ solution that the logarithmic term is

indeterminate at $x > 0.25$, which would prevent application of the equations all the way to the upper phase boundary of $\langle UO_{2+x} \rangle$.

The $[UO_2]$-$[U_3O_7]$ representation was used in a much more extensive least-squares analysis of the data base. The equation for this can be arranged in the form

$$RT \ln (p^*_{O_2}) - 2RT \ln \frac{x(1-2x)^2}{(1-3x)^3} = \Delta H^o_{rxn} - T\Delta S^o_{rxn} + E \frac{2 - 12x + 12x^2}{(1-2x)^2} . \quad (13)$$

It was applied to all data for which $RT \ln(p^*_{O_2})$ was more positive than -260 kJ/mol. This amounted to 1145 sets of T-x-$\ln(p^*_{O_2})$ values. The least-squares analysis gave the values $\Delta H^o_{rxn} = -297700$ J/mol, $\Delta S^o_{rxn} = -117$ J·mol^{-1}·K^{-1}, and E = -2632 J/mol. Since E was small, the data base was reanalyzed assuming E = 0, giving $\Delta H^o_{rxn} = -312807$ J/mol and $\Delta S^o_{rxn} = -126$ J·mol^{-1}·K^{-1}. As will be shown later, the effects of the E term appeared inconsequential, and the latter enthalpy and entropy values were utilized.

The thermodynamic values for the $[UO_2]$-$[U_3O_7]$ representation were used to calculate the values of x at the phase boundary with $\langle U_4O_9 \rangle$. As will be shown in section 4.4, the $[UO_2]$-$[U_3O_7]$ solution is applicable at the phase boundary for O/U > 2.05. The calculated values of x were then compared with the values of Grønvold,[42] which appear to be representative of several investigations. The relevant equilibrium is

$$[UO_2] + [U_3O_7] \leftrightarrows \langle U_4O_9 \rangle . \quad (14)$$

Reference 43 gives tabulated values for the standard free energy of formation for $\langle UO_2 \rangle$ and $\langle U_4O_9 \rangle$. The values at 600 and 1200 K were used to give the relationships

$$\Delta G_f^o\langle UO_2 \rangle \text{ (J/mol)} = -1080000 + 169.0T \quad (400 < T < 1400 \text{ K}) , \tag{15}$$

and

$$\Delta G_f^o\langle U_4O_9 \rangle \text{ (J/mol)} = -4489000 + 739.1T \quad (400 < T < 1400 \text{ K}) . \tag{16}$$

The equivalent expression for $\langle U_3O_7 \rangle_{fcc}$ was derived from eq. (13), for which ΔG_{rxn}^o (J/mol) = $-312800 + 126T$, which is equivalent to $2\Delta G_f^o\langle U_3O_7 \rangle_{fcc} - 6\Delta G_f^o\langle UO_2 \rangle$. This and eq. (15) lead to

$$\Delta G_f^o\langle U_3O_7 \rangle_{fcc} \text{ (J/mol)} = -3396400 + 569.9T . \tag{17}$$

With this information, the free energy difference for reaction (16) is ΔG_{rxn}^o (J/mol) = $-12600 + 0.3T$, and eqs. (5), (6), and (14-17) lead to

$$\Delta G_{rxn}^o = 0 = -12600 + 0.3T - RT \ln \frac{x(1-3x)}{(1-2x)^2} . \tag{18}$$

The Newton-Raphson technique (see Appendix 1) was used to solve for values of x at $400 < T < 1400$ K. At a given x value, the present analysis predicted a phase boundary lying about 200 K lower than observed.[40] However, all could be brought into essentially perfect agreement by using an enthalpy of -16000 J/mol in eq. (18). This minor correction of -3400 J/mol is about 20% of the uncertainty of the $\Delta H_{f,298}^o$ value for $\langle U_4O_9 \rangle$,[44] and it is suggested that, for the phase boundary calculation, eq. (18) be made more negative by this amount. The final form of the $[UO_2]$-$[U_3O_7]$ representation is thus:

$$RT \ln (p^*_{O_2}) \text{ (J/mol)} = -312800 + 126T + 2RT \ln \frac{x(1-2x)^2}{(1-3x)^3}, \quad (19a)$$

$$\Delta\bar{G}[UO_2] \text{ (J/mol)} = -1080000 + 169.0T + RT \ln \frac{1-3x}{1-2x}, \quad (19b)$$

and

$$\Delta\bar{G}[U_3O_7] \text{ (J/mol)} = -3396400 + 569.9T + RT \ln \frac{x}{1-2x} \quad (19c)$$

Four other techniques were used to compare the results of the least-squares fit with the raw data base and with the results of other fits to the data. The first technique was the least-squares determination of the slope as well as ΔH^o_{rxn}, ΔS^o_{rxn}, and E, the second was the statistical definition of the standard deviation, the third was a plot of fitted oxygen potential minus observed oxygen potential versus temperature (a residuals plot), and the fourth was a transformation of all the data to 1500 K. To determine the slope by the least-squares method, the ln term in eq. (13) was placed on the right-hand side and resulted in a slope of 1.95. This value is within 3% of the theoretical value of two and helps confirm that the model does represent the behavior of the data. The values of the standard deviations of the fits with and without E showed that including E reduced the standard deviation from 8650 J/mol to 8250 J/mol, or only about 5%. The residuals plot appeared the same whether or not the E term was included, and also illustrated no trend of the residuals with temperature, which indicates that the fit adequately represents the temperature dependence of the data.

Figure 3, the transformation of all the data to 1500 K, was accomplished with the use of eq. (13) divided by RT. After writing one equation at 1500 K, the second at temperature T, and subtracting the second from the first, one obtains the general equation

$$\ln (p^*_{O_2})_{1500K} = \ln (p^*_{O_2})_T + 1/R\left[\Delta H^o_{rxn} + E\ \frac{2 - 12x + 12x^2}{(1 - 2x)^2}\right]\left[\frac{1}{1500} - \frac{1}{T}\right] \quad (20)$$

Choosing first $\Delta H^o_{rxn} = -312807$ J/mol and E = 0, the right-hand side of eq. (20) was evaluated from each experimental T-x-$\ln(p^*_{O_2})$ data set, thus giving the $\ln(p^*_{O_2})$ values transformed to 1500 K. Again using E = 0, these values are plotted as the ordinate in fig. 3 versus the abscissa values calculated from the general function

$$\ln\left[\frac{x(1-2x)^2}{(1-3x)^3}\right] + \frac{E\ (2-12x + 12x^2)}{2R\ 1500\ (1-2x)^2} . \quad (21)$$

Also shown in fig. 3 is the line representing the behavior predicted at 1500 K from the least-squares fit of the data base; this line has a slope of 2. An analogous plot with $\Delta H^o_{rxn} = -297700$ and E = -2632 J/mol was not discernibly better than that shown in fig. 3. Consideration of all the factors described above led to the conclusion that the E term was unimportant and could be assumed to be zero.

The process described above was repeated in its entirety for the $[UO_2]$-$[U_{10/3}O_{23/3}]$ solution. The least-squares determination of the slope gave 1.74, as opposed to the theoretical

value of 2 and the value of 1.95 obtained from the $[UO_2]$-$[U_3O_7]$ solution. Comparison of all the other results revealed no discernible improvement in the fit of the data over that obtained with the $[UO_2]$-$[U_3O_7]$ solution. It was thus dropped from further consideration.

4.3 $\langle UO_{2+x} \rangle$, low hyperstoichiometry

In this section the hyperstoichiometric data lying below an oxygen potential of -260 kJ/mol will be analyzed. There are some indications in the raw data base that the slope of the $\ln(p^*_{O_2})$-$\ln(x)$ plot in this region may be temperature dependent. To explore this possibility, the data were analyzed utilizing the equation

$$\ln(p^*_{O_2}) = a/T + b + c \ln(x) + eT \ln(x) \quad . \qquad (22)$$

The least-squares analysis of the approximately 200 T-x-$\ln(p^*_{O_2})$ values gave values of a, b, c, and e, with the term e being used to reveal any temperature dependence of the slope, c. The analysis determined a slope of 4.21, which is within 6% of 4.00, while the temperature dependence contributed only about a 1% variation in the slope, that is, the slope was independent of temperature.

Two solid solutions were considered for this region, $[UO_2]$-$[U_2O_{4.5}]$ and $[UO_2]$-$[U_{1.5}O_{3.5}]$. These choices were made on the assumption that the O/U ratio of the solute oxide should be that of a known U-O compound and that the ratio should possibly be equal to or less than that for the $[U_3O_7]$ used in the more hyperstoichiometric region. The particular oxide formulations used here, $[U_2O_{4.5}]$ and $[U_{1.5}O_{3.5}]$, were chosen so that the equations shown below would give the observed slope of 4. The

least-squares analysis was applied to the data for which O/U > 2 and the oxygen potential was less than -260 kJ/mol. For the $[UO_2]$-$[U_2O_{4.5}]$ solution, the equation is

$$RT \ln (p^*_{O_2}) \text{ (J/mol)} = -360000 + 214T + 4RT \ln \frac{2x(1-2x)}{(1-4x)^2} , \quad (23a)$$

and the partial Gibbs free energy relations are

$$\Delta\bar{G}[UO_2] \text{ (J/mol)} = -1080000 + 169.0T + RT \ln \frac{1-4x}{1-2x} , \quad (23b)$$

and

$$\Delta\bar{G}[U_2O_{4.5}] \text{ (J/mol)} = -2250000 + 391.4T + RT \ln \frac{2x}{1-2x} , \quad (23c)$$

while for the $[UO_2]$-$[U_{1.5}O_{3.5}]$ solution,

$$RT \ln (p^*_{O_2}) \text{ (J/mol)} = -360000 + 214T + 4RT \ln \frac{2x(1-x)^{0.5}}{(1-3x)^{1.5}} . \quad (24)$$

An extensive comparison of the two with the data revealed no difference between them. Arbitrarily, the $[UO_2]$-$[U_2O_{4.5}]$ solution is used to represent the data in this region.

The predictions of the $[UO_2$-$U_2O_{4.5}]$ representation compare reasonably well with the low-x data, as seen in fig. 3. Again, using the procedures outlined in the derivation of eq. (20), all the data were transformed to 1500 K utilizing the equation

$$\ln(p^*_{O_2})_{1500K} = \ln(p^*_{O_2})_T - \frac{360000}{R}\left(\frac{1}{1500} - \frac{1}{T}\right) \quad (25)$$

and plotted versus the function

$$\ln \frac{2x(1-2x)}{(1-4x)^2} - \ln(2) . \quad (26)$$

Here, the factor ln(2) is subtracted from the first term so that the data would join smoothly along the abscissa with the data plotted via the $[UO_2]$-$[U_3O_7]$ representation. [At low x, the logarithmic term of the latter representation reduces to approximately ln(x), while that for the $[UO_2]$-$[U_2O_{4.5}]$ representation reduces to approximately ln(2x).]

Neither of these two representations of the data predicted the values of x for the $\langle UO_{2+x}\rangle$-$\langle U_4O_9\rangle$ two-phase region. Both are applicable at approximately O/U $\leq$ = 2.06, as will be shown in section 4.7. At the boundary, the equilibria $2[U_2O_{4.5}] \leftrightarrows \langle U_4O_9\rangle$ and $[UO_2] + 2[U_{1.5}O_{3.5}] \leftrightarrows \langle U_4O_9\rangle$ are applicable and both led to large x values at low temperatures and small values at high temperatures, which is opposite to the experimental behavior.[42] Additionally, calculations for these equilibria demonstrated that, in order to bring the model into agreement with the phase boundary, the ΔH^o_{rxn} value would have to be changed from 11000 to -76500 J/mol, while the ΔS^o_{rxn} value would have to be changed from -43.7 to 68.74 $J \cdot mol^{-1} \cdot K^{-1}$. Such adjustments are unrealistic.

4.4 The boundary between the two $\langle UO_{2+x}\rangle$ regions

The location of the boundary between the two hyperstoichiometric regions can be calculated from the results in sections 4.2 and 4.3. For the boundary between the $[UO_2]$-$[U_3O_7]$ and $[UO_2]$-$[U_2O_{4.5}]$ systems, eq. (23a) is subtracted from eq. (19a) and the terms rearranged to give

$$0 = \frac{5677}{T} - 10.5 + 2 \ln \frac{(1-4x)^4}{4x(1-3x)^3} . \qquad (27)$$

This equation was solved for x at a given temperature by the Newton-Raphson iterative technique, and then the value of x was substituted into eq. (23a) to calculate $\ln(p^*_{O_2})$ and the oxygen potential at that temperature. Figure 4 illustrates the boundary and permits comparison with several sets of experimental data. The oxygen potential of the boundary is represented by the equation

$$RT \ln (p^*_{O_2}) \text{ (J/mol)} = -266700 + 16.5T \ . \qquad (28)$$

4.5 $\langle UO_{2-x} \rangle$

The hypostoichiometric data consisted of about 220 T-x-$p^*_{O_2}$ values. These data were difficult to analyze by the current methods because of two factors: first, the complexity of the original experiments at high temperatures and very low oxygen potentials led to considerable scatter in the data; second, there were little data at O/U < 1.9 or x > 0.1. It was demonstrated above that x values considerably larger than 0.1 were necessary to distinguish the best solute species. The single very substoichiometric data set is that of Ackermann et al.,[22] but it is not isothermal and cannot be used to plot the data in the manner used in fig. 2. Fortunately, the x dependence for the $\{U\}$-$\langle UO_{2-x} \rangle$ two-phase region could be used to help define the best fit of the data.

The analysis commenced by determining the slope of the $\ln(p^*_{O_2})$-ln(x) relationship, eq. (7). The slope was dependent upon which portion of the data base was included. For the entire data base, 1.99993 > O/U > 1.692, the slope was -2.27; with the upper O/U cutoff at 1.999, the slope was -2.33, and for 1.99, it was -3.16.

It was thus decided to explore several solid-solution representations that would have slopes of -2, -3, and -4. The U-O phase diagram provides little guidance for possible solutes, since there are no oxides lying between uranium and $\langle UO_{2-x} \rangle$, but uranium is clearly suggested as a solute. Trivalent uranium suggests a solute oxide having an O/U ratio of 1.5, and the presence of [UO] in extensive solution in [UC][45] suggests an O/U equaling 1.0. The following equilibria can thus be written for O/U = 1.5:

$$2[U_2O_3] + (O_2) = 4[UO_2], \text{ slope} = -2; \quad (29)$$

$$3[U_{1.33}O_2] + (O_2) = 4[UO_2], \text{ slope} = -3; \quad (30)$$

and

$$4[UO_{1.5}] + (O_2) = 4[UO_2], \text{ slope} = -4; \quad (31)$$

while for O/U = 1.0,

$$2[UO] + (O_2) = 2[UO_2], \text{ slope} = -2; \quad (32)$$

$$3[U_{0.67}O_{0.67}] + (O_2) = 2[UO_2], \text{ slope} = -3; \quad (33)$$

and

$$4[U_{0.5}O_{0.5}] + (O_2) = 2[UO_2], \text{ slope} = -4; \quad (34)$$

and for the solute uranium,

$$2[U_{0.5}] + (O_2) = [UO_2], \text{ slope} = -2; \quad (35)$$

$$3[U_{0.33}] + (O_2) = [UO_2], \text{ slope} = -3; \quad (36)$$

and

$$4[U_{0.25}] + (O_2) = [UO_2], \text{ slope} = -4. \quad (37)$$

All the equilibria were analyzed in considerable detail. This included plotting all the data transformed to 2400 K, as shown in fig. 5 for the $[UO_2]$-$[U_{1/3}]$ solution. It was particularly clear that the solutions for which the slope was -3 fit the data best. This was especially true for the data of Ackermann et al.[22] In fig. 5

their data fell amidst the data of the other investigators, whereas in a similar figure plotted according to the system of eq. (35) it was below and to the left of the rest, and for the system of eq. (37) it was above and to the right. It was also apparent that at any given slope, there was no discernible difference in the goodness of the fit as a function of the O/U ratio of the models used for that particular slope. Nevertheless, the three solutions for which the slope is -3 were all fitted to the entire data base (O/U < 2) and gave the following equations, which are to be modified later:

$[UO_2\text{-}U_{1/3}]$ solution,

$$RT \ln (p^*_{O_2}) \text{ (J/mol)} = -1230100 + 225.7T + 26900 \frac{3x+1.5x^2-3}{(1+x)^2} - 3RT \ln \frac{1.5x}{(1+x)^{2/3}(1-0.5x)^{1/3}} ; \quad (38)$$

$[UO_2]\text{-}[U_{2/3}O_{2/3}]$ solution,

$$RT \ln (p^*_{O_2}) \text{ (J/mol)} = -1226800 + 229.4T + 30285 \frac{6x-1.5x^2-3}{(1+0.5x)^2} - 3\,RT \ln \frac{1.5\ x}{(1+0.5x)^{1/3}(1-x)^{2/3}} ; \quad (39)$$

and

$[UO_2]\text{-}[U_{4/3}O_2]$ solution,

$$RT \ln (p^*_{O_2}) \text{ (J/mol)} = -1228300 + 238.2T + 34845 \frac{12x-3x^2-3}{(1.-0.5x)^2} -3\,RT \ln \frac{1.5x(1-0.5x)^{1/3}}{(1-2x)^{4/3}} . \quad (40)$$

In addition to the above three equations, another set of three equations were forced to fit the data of Ackermann et al.[22] Their data are the only T-x-$\overset{*}{p}_{O_2}$ data at the phase boundary with uranium and are the only data for which the x dependence of the interaction terms is significant. The least-squares fitting process began for the total data base by assuming the interaction term was zero and solving for the enthalpy and entropy values only. It was noted that, for a given model, the entropy term remained nearly constant whether or not the interaction term was included. Then, using this entropy value as a known, the data of Ackermann et al.[22] was fitted to give the interaction parameter coefficient as well as a new enthalpy value. In this way, their data could be fitted almost perfectly.

Use of any of the six representations to calculate values of x for the $\{U\}$-$\langle UO_{2-x}\rangle$ two-phase region led to x values two to three times larger than those measured, and the fitting procedure was modified. Equations (38-40) are obviously very similar and fit the data equally well as far as could be determined, but the $[UO_2]$-$[U_{1/3}]$ solution is preferred. It is the most straightforward to apply to other thermodynamic analyses because all the thermodynamic data for uranium are known, whereas they are not for uranium monoxide and sesquioxide. Thus, in the $\{U\}$-$\langle UO_{2-x}\rangle$ two-phase region, one has the equilibrium

$$1/3\{U\} \rightleftharpoons [U_{1/3}] \ , \qquad (41)$$

for which the free energy relation is generally

$$0 = \Delta H^{o}_{rxn} - T\Delta S^{o}_{rxn} + RT \ln \frac{1.5x}{1+x} + E\left(\frac{1-0.5x}{1+x}\right)^2 . \qquad (42)$$

The chemical activity of {U} is assumed to be unity, and the free energy of formation {U} is by definition, zero. Thus, the enthalpy and entropy terms in eq. (42) are those for $\{U_{1/3}\}_{fcc}$, which were determined in the following manner. Several different least-squares fitting procedures were used to obtain values of ΔH^{o}_{rxn}, ΔS^{o}_{rxn}, and E for eq. (38). The enthalpy and entropy values represent those for the difference $\Delta G^{o}_{f}\langle UO_2\rangle - 3\Delta G^{o}_{f}\langle U_{1/3}\rangle_{fcc}$. Values of $\Delta G^{o}_{f}\langle UO_2\rangle$ are given in ref. 43 and can be represented by -1079700 + 170.5T J/mol for the temperature range of the UO_{2-x} data. Thus, the Gibbs free energy of formation for uranium in solution was calculated, which gave the required enthalpy and entropy values for eq. (42). By far, the best agreement at the phase boundary was obtained by fitting all the data without an interaction parameter. For example, at 1872, 2347, and 2700 K the calculated values of x were 0.058, 0.165, and 0.301, respectively. These compare with 0.043, 0.179, and 0.330, respectively, from the assessment shown in fig. 2 of Green and Leibowitz.[46] Thus, the $\langle UO_{2-x}\rangle$ region appears to be best represented by the $[U_{1/3}]$-$[UO_2]$ solution for which the final equations are

$$RT \ln (p^{*}_{O_2}) \text{ (J/mol)} = -1300000 + 225.7T - 3RT \ln \frac{1.5x}{(1+x)^{2/3}(1-0.5x)^{1/3}} , \qquad (43a)$$

$$\Delta\bar{G}[UO_2] \text{ (J/mol)} = -1079700 + 170.5T + RT \ln \frac{1-0.5x}{1+x} , \qquad (43b)$$

and

$$\Delta\bar{G}[U_{1/3}]\ (J/mol) = 73433 - 18.4T + RT \ln \frac{1.5x}{(1+x)} \quad (43c)$$

4.6 Oxygen potential for $\langle UO_2 \rangle$

The oxygen potential for exactly stoichiometric $\langle UO_2 \rangle$ can be obtained from eqs. (19a), (23a), and (43a). Exact stoichiometry can be defined as the condition where the hyperstoichiometry equals the hypostoichiometry. Also, the nonstoichiometry is very small. Thus, eq. (23a) can be written in the form

$$RT \ln (p^*_{O_2})\ (J/mol) = -360000 + 214T + 4RT \ln(2) + 4RT \ln(x) \quad (44)$$

and eq. (43a) becomes

$$RT \ln (p^*_{O_2})\ (J/mol) = -1300000 + 225.7T - 3RT \ln(1.5) - 3RT \ln(x) . \quad (45)$$

Upon eliminating the terms in ln(x) and rearranging, the desired definition becomes

$$RT \ln (p^*_{O_2})\ (J/mol) = -897000 + 224.8T \quad (T < 3015) . \quad (46)$$

The temperature limit of 3015 K results from the intersection of the oxygen potential for exact stoichiometry with that for the $[UO_2]$-$[U_3O_7]$-$[U_2O_{4.5}]$ boundary, eq. (28). Above 3015 K, the $[UO_2]$-$[U_3O_7]$ and $[UO_2]$-$[U_{1/3}]$ representations can be combined similarly to give the definition of exact stoichiometry up to the melting temperature of $\langle UO_2 \rangle$,

$$RT \ln (p^*_{O_2})\ (J/mol) = -707700 + 161.8T \quad (3015 < T < 3120\ K) . \quad (47)$$

4.7 Oxygen potential at $\langle UO_{2\pm x}\rangle$ phase boundaries

The oxygen potential of the $\langle UO_{2+x}\rangle$-$\langle U_4O_9\rangle$ two-phase region was calculated from the results given in section 4.2. Equation (18), with an enthalpy value of -16000 J/mol, was used to calculate x values of 0.083, 0.155, and 0.206 at 800, 1100, and 1300 K, respectively. The oxygen potential at these values is then calculated from eq. (19a) and fitted to give the oxygen potential of the phase boundary from 715 to 1400 K,

$$RT \ln (p^*_{O_2}) \text{ (J/mol)} = -390200 + 189.6T \ . \quad (48)$$

The lower limit of 715 K comes from the intersection of eq. (48) with eq. (28), which occurs at O/U ≈ 2.06. Equation (48) agrees within a few percent of that from eq. (5) of a publication of Blackburn.[4]

The oxygen potential of the $\langle UO_{2+x}\rangle$-$\{UO_{2+x'}\}$ two-phase region was estimated in the following manner. The experiments of Latta and Fryxell[47] gave $\langle UO_{2.1}\rangle$ for the solidus composition at 2820 K, and eq. (19a) gives an oxygen potential of -36202 J/mol. For $\langle UO_2\rangle$ at 3120 K, the melting temperature, eq. (47) gives an oxygen potential of -202884 J/mol. Assuming linearity of oxygen potential with temperature leads to

$$RT \ln (p^*_{O_2}) \text{ (J/mol)} = 1530600 - 556 \ T \ . \quad (49)$$

The $\langle UO_{2-x}\rangle$ equilibria with liquid uranium containing dissolved oxygen has two regions lying on either side of the 2700 K monotectic.[46] Below 2700 K, the x values for the phase boundary were given in section 4.5 at three temperatures. These data were used in eq. (43a) to calculate the oxygen potential at T <2700 K and led to

$$RT \ln (p^*_{O_2}) \text{ (J/mol)} = -1063400 + 160.9\ T \ . \quad (50)$$

Above 2700 K, the oxygen potentials at 2700 and 3120 K were used similarly to give for that temperature range

$$RT \ln (p^*_{O_2}) \text{ (J/mol)} = -3367600 + 1014T \ . \quad (51)$$

5. DISCUSSION AND CONCLUSIONS

Figure 6 illustrates the T-x-RT $\ln(p^*_{O_2})$ dependence predicted from the present analysis and permits a qualitative comparison of the prediction with the data. The $\langle UO_{2+x} \rangle$ behavior was calculated from the two different hyperstoichiometric solutions, eqs. (19a) and (23a), which intersect at their mutual boundary, eq. (28). The behavior of $\langle UO_{2-x} \rangle$ is represented by eq. (43a). Exact stoichiometry is defined by eqs. (46) and (47), and it can be seen from fig. 6 that the adjacent hyperstoichiometry and hypostoichiometry intersect properly at stoichiometry. The $\langle UO_{2+x} \rangle$-$\{UO_{2+x'}\}$ two-phase region calculated from eq. (49) is illustrated, as are the two $\langle UO_{2-x} \rangle$ phase boundaries with U-O liquids calculated from eqs. (50) and (51).

Figure 3 illustrates that some of the $\langle UO_{2+x} \rangle$ data sets disagree markedly with the majority. Those data in disagreement were not included in the present numerical analysis, as was noted at the beginning of section 4. For $\langle UO_{2-x} \rangle$, all of the data, except Swanson's,[31] appeared to be in reasonable agreement, as is shown in fig. 5; Swanson's data was off-scale on the positive side. Tetenbaum and Hunt's[20] data exhibited the characteristic rapid rise in oxygen potential at O/U = 2.006, rather than the usually observed O/U = 2. The present model does not reflect the behavior of Tetenbaum and

Hunt's data. However, if all their O/U values would have been decreased by 0.006, they would have agreed much more closely with the other data shown in figs. 3 and 5.

The model proposed by Blackburn[48] was compared with the present results. For $\langle UO_{2-x} \rangle$, his eq. (11) was used to give the behavior shown in fig. 5, while for $\langle UO_{2+x} \rangle$ his eq. (17a) gave the results shown in fig. 3. His equation for hyperstoichiometry includes an empirical polynomial term that permits a fit of the data for $O/U > 2.1$. It can be seen from fig. 3 that his equation adequately represents the data in the same region that the present $[UO_2]$-$[U_3O_7]$ representation is used, but the present representation needs no empirical adjustment at $O/U > 2.1$. Figure 3 also illustrates that Blackburn's model apparently does not represent the data at small hyperstoichiometries. For $\langle UO_{2-x} \rangle$, fig. 5 illustrates that Blackburn's model generally appears to lie on the low side of the data, but it does agree with the data at the lower phase boundary, which he used to obtain his ΔH^{o}_{rxn} and ΔS^{o}_{rxn}. Blackburn's definition of the oxygen potential for exactly stoichiometric $\langle UO_2 \rangle$ was obtained by combining his eqs. (11) and (23) to give $RT \ln(p^{*}_{O_2}) = -787750 + 167.0T$ J/mol. A more recent evaluation of exact stoichiometry by Hyland[49] gives a nearly identical equation. These can be compared with that from eqs. (46) and (47), which give an oxygen potential 52 kJ/mol more negative at 1000 K, exact agreement at 1916 K, and 64 kJ/mol more positive at the melting temperature, 3120 K. Some of the disagreement between the present model and Blackburn's is undoubtedly the result of the

poor fit of the near-stoichiometric data by Blackburn's model (figs. 3 and 5). Additionally, Breitung[50] calculated the oxygen potential for stoichiometric $\langle UO_2 \rangle$; data in his table 3 lead to $RT \ln(p^*_{O_2}) = -766500 + 157.3T$ J/mol, a result closer to those of Blackburn[48] and Hyland[49] than to the present analysis.

It is interesting to note that Fink et al.[51] analyzed the enthalpy data for $\langle UO_2 \rangle$ and concluded that 2670 K is the temperature for a significant transition in the enthalpy behavior. This transition temperature compares with the present 3015 K for the intersection of the $[UO_2]$-$[U_3O_7]$, $[UO_2]$-$[U_2O_{4.5}]$, and $[UO_2]$-$[U_{1/3}]$ solutions. It is interesting to speculate whether the coincidence of the several solid solutions is relevant to the enthalpy transition for $\langle UO_2 \rangle$.

The solid solutions treated here lead to a useful mathematical representation of the T-x-$p^*_{O_2}$ behavior, but undoubtedly provide little or no insight into the actual structure of the defected fluorite lattice, as was noted in the introduction.

ACKNOWLEDGMENTS

The authors express their appreciation to D. J. Pruett and J. Brynestad, for valuable discussions. We also thank M. LaRoche and D. Depaoli who were instrumental in retrieving data from the literature, and B. C. Drake who patiently helped prepare the manuscript.

APPENDIX 1. THE NEWTON-RAPHSON TECHNIQUE

An adaptation of the Newton-Raphson technique proved invaluable for computer solution of the value of x, i.e., the root of the equation, at a given $\ln(p^*_{O_2})$. Writing any given expression as $F(x) = 0$, the technique states that, if x_i is an approximation of a root, an improved approximation is given by

$$x_{i+1} = x_i - tF(x_i)/F'(x_i) \qquad (a1)$$

where the prime indicates the derivative and where t is usually unity. Here it was found that allowing $t = 0.01\ i^2$, but not allowing t to grow to be greater than unity, helped speed convergence to the root. The derivative was approximated by

$$F'(x_i) = [F(x_i+\delta) - F(x_i-\delta)]/2\delta \qquad (a2)$$

where $\delta = 0.001\ x_i$ was usually a sufficiently small increment in x_i. Smaller values were sometimes needed for rapidly changing functions. The root was obtained when the absolute value of $1-x_{i+1}/x_i$ became equal to or less than the multiplier of x_i in the equation for δ, in this example 0.001. The starting value, x_1, was typically set to a value smaller than the expected root, and in general $x_1 = 10^{-8}$ was used. In very complex equations, however, x_1 needed to be within a few percent or less of the expected value. The convergence process can be monitored during computations to insure that a proper root is being determined by observing the values of x_i, $F(x_i)$ (which approaches zero at convergence), and $F'(x_i)$ (which changes sign at convergence).

REFERENCES

1. M. Hoch and F.J. Furman, in: Proc. Symp. on Thermodyn. 1965, Vienna, Vol. II (IAEA, Vienna, 1966) pp. 517-32.

2. J.-F. Babelot, M. Hoch and R.W. Ohse, High Temp.-High Pressures 1 (1982) 431.

3. S. Aronson and J. Belle, J. Chem. Phys. 29 (1958) 151.

4. P. E. Blackburn, J. Phys. Chem. 62 (1958) 897.

5. L.E.J. Roberts and A.J. Walter, Atomic Energy Research Establishment, Harwell, England, Harwell Report AERE-R 3345 (1960).

6. E. Aukrust, T. Forland and K. Hagemark, in: Proc. Symp. Thermodyn. Nucl. Mater. Vienna (IAEA, Vienna, 1962) pp. 713-22.

7. K. Kiukkola, Acta Chem. Scand. 16 (1962) 327.

8. T.L. Markin and R.J. Bones, Atomic Energy Research Establishment, Harwell, England, Harwell Report AERE-R 4042 (1962).

9. T.L. Markin and R.J. Bones, Atomic Energy Research Establishment, Harwell, England, Harwell Report AERE-R 4178 (1962).

10. T.L. Markin, L.E.J. Roberts and A. Walter, in: Proc. Symp. Thermodyn. Nucl. Mater. Vienna (IAEA, Vienna, 1962) pp. 693-711.

11. A.M. Anthony, R. Kiyoura and T. Sata, J. Nucl. Mater. 10 (1963) 8.

12. A.T. Chapman and R.E. Meadows, J.Am. Ceram. Soc. 47 (1964) 614.

13. P. Gerdanian and M. Dodé, J. Chim. Phys. Phys.-Chim. Biol. 62 (1965) 171.

14. T.L. Markin and E.J. McIver, in: Proc. Conf. Plutonium 1965 London (Inst. of Metals, London, 1967) pp. 845-57.

15. E.A. Aitken, H.C. Brassfield and R.E. Fryxell, in: Proc. Symp. Thermodyn. Vienna 1966 (IAEA, Vienna, 1966) pp. 435-53.

16. K. Hagemark and M. Broli, J. Inorg. Nucl. Chem. 38 (1966) 2837.

17. A. Kotlar, P. Gerdanian and M. Dodé, J. Chim. Phys. Phys.-Chim. Biol. 64 (1967) 1135.

18. T.L. Markin, V.J. Wheeler and R.J. Bones, J. Inorg. Nucl. Chem. 30 (1968) 807.

19. A. Pattoret, J. Drowart and S. Smoes, in: Proc. Symp. Thermodyn. Nucl. Mater. Vienna 1967 (IAEA, Vienna, 1968) pp. 613-36.

20. M. Tetenbaum and P.D. Hunt, J. Chem. Phys. 49 (1968) 4739.

21. C. Thomas, P. Gerdanian and M. Dodé, J. Chim. Phys. Phys.-Chim. Biol. 65 (1968) 1349.

22. R. J. Ackermann, E.G. Rauh and M.S. Chandrasekharaiah, J. Phys. Chem. 73 (1969) 762.

23. V.J. Wheeler, J. Nucl. Mater. 39 (1971) 315.

24. V.J. Wheeler and I.G. Jones, J. Nucl. Mater. 42 (1972) 117.

25. N.A. Javed, J. Nucl. Mater. 43 (1972) 219.

26. D.I. Marchidan and S. Matei, Rev. Roum. Chim. 17 (1972) 195.

27. D.I. Marchidan and S. Matei, Rev. Roum. Chim. 17 (1972) 1487.

28. M.G. Adamson and R.F.A. Carney, J. Nucl. Mater. 54 (1974) 121.

29. Y. Saito, J. Nucl. Mater. 51 (1974) 112.

30. D.I. Marchidan and S. Tanasescu, Rev. Roum. Chim. 20 (1975) 1365.

31. G.C. Swanson, Los Alamos National Laboratory, Los Alamos Report LA-6083-T (1975).

32. G.R. Chilton and I.A. Kirkham, in: Proc. Conf. Plutonium 1975 and Other Actinides Baden Baden (North-Holland, Amsterdam, 1976) pp. 171-80.

33. W.G. Jocher, Kernforschungszentrum Karlsruhe GmbH, F.R.G., Report KfK 2518, corrected (1978).

34. A.T. Chapman, J. Brynestad and G.W. Clark, High Temp.–High Pressures 12 (1980) 447.

35. V.G. Baranov and Y.G. Godin, At. Energy Engl. Transl. 51 (1982) 633.

36. K. Une and M. Oguma, J. Nucl. Mater. 110 (1982) 215.

37. F. Schleifer, A. Naoumidis and H. Nickel, J. Nucl. Mater. 115 (1983) 143.

38. M. Ugajin, J. Nucl. Sci. Technol. 20 (1983) 288.

39. K. Une and M. Oguma, J. Nucl. Mater. 115 (1983) 84.

40. T.B. Lindemer and T.M. Besmann, Oak Ridge National Laboratory, Oak Ridge Report ORNL/TM-8998 (1984).

41. L.S. Darken and R.W. Gurry, Physical Chemistry of Metals (McGraw-Hill, New York, 1953) pp. 266-69.

42. F. Grønvold, J. Inorg. Nucl. Chem. 1 (1955) 357.

43. L.B. Pankratz, Thermodynamic Properties of the Elements and Oxides, U.S. Dept. Interior Bureau of Mines Bulletin 672 (U.S. Gov't. Printing Office, Washington, D.C., 1982).

44. O. Kubaschewski and C.B. Alcock, Metallurgical Thermochemistry, 5th Ed. (Pergamon Press, Oxford, England, 1979) Table A.

45. T. M. Besmann, J. Am. Ceram. Soc. 66 (1983) 353.

46. D.W. Green and L. Leibowitz, J. Nucl. Mater. 105 (1982) 184.

47. R.E. Latta and R.E. Fryxell, J. Nucl. Mater. 35 (1970) 195.

48. P.E. Blackburn, J. Nucl. Mater. 46 (1973) 244.

49. G.J. Hyland, Dept. of Physics. U. of Warwick, England, Report dated 23 Feb. 1984.

50. W. Breitung, Kernforschungszentrum Karlsruhe Gmbh, F.R.G., Report KfK 2901 (1975).

51. J.K. Fink, M.G. Chasanov and L. Leibowitz, J. Nucl. Mater. 102 (1981) 17.

TABLE 1
$UO_{2\pm x}$ data base

Authors	Reference	Year	Temperature (K)	Oxygen-to-Metal Ratio	Number of Points
Aronson and Belle	3	1958	1150–1350	2.0130–2.2030	52
Blackburn	4	1958	1239–1399	2.13–2.23	45
Roberts and Walter	5	1960	1372–1695	2.0094–2.2300	102
Aukrust, Forland, and Hagemark	6	1962	1373–1673	2.0008–2.2283	53
Kiukkola	7	1962	1073–1473	2.0140–2.2390	44
Markin and Bones	8	1962	735–1387	2.0120–2.1880	185
Markin and Bones	9	1962	923–1297	2.0000–2.0327	191
Markin, Roberts, and Walter	10	1962	765–1350	2.0129–2.1873	44
Anthony, Kiyoura, and Sata	11	1963	1500–2086	2.1203–2.2728	42
Chapman and Meadows	12	1964	1268–1773	2.0200–2.2200	14
Gerdanian and Dodé	13	1965	1176–1373	2.0041–2.1852	99
Markin and McIver	14	1965	1173	2.0018–2.0770	6
Aitken, Brassfield, and Fryxell	15	1966	2023–2873	1.8702–1.9942	17
Hagemark and Broli	16	1966	1173–1773	2.0020–2.2250	51
Hoch and Furman	1	1966	1173	2.0070–2.0120	4
Kotlar, Gerdanian, and Dodé	17	1967	1355–1423	2.1977–2.2451	57
Markin, Wheeler, and Bones	18	1968	1600–2400	1.9170–2.0750	36
Pattoret, Drowart, and Smoes	19	1968	1807–2477	1.9000–2.0000	44
Tetenbaum and Hunt	20	1968	2080–2705	1.8740–2.0186	108
Thomas, Gerdanian, and Dodé	21	1968	1446–1696	2.0014–2.0427	81
Akermann, Rauh, and Chandrasekharaiah	22	1969	1872–2529	1.6921–1.9607	10
Wheeler	23	1971	1800–2000	1.9860–2.0000	15
Wheeler and Jones	24	1972	1950	1.9967–2.0062	11
Javed	25	1972	1873–2173	1.9600–2.0000	31
Marchidan and Matei	26	1972	1073–1373	2.0400–2.2100	19
Marchidan and Matei	27	1972	1173–1373	2.18	5
Adamson and Carney	28	1974	1633–1773	2.0000–2.0690	4
Saito	29	1974	973–1473	2.0410–2.1870	55
Marchidan and Tanasescu	30	1975	1273–1373	2.20	3
Swanson	31	1975	1073–1569	1.9988–2.0101	41
Chilton and Kirkham	32	1976	1518–1823	2.0001–2.1260	48
Jocher	33	1978	1073–1473	2.02	5
Chapman, Brynestad, and Clark	34	1980	1933	2.0000–2.0757	8
Baranov and Godin	35	1982	976–1273	1.9991–2.0039	75
Une and Oguma	36	1982	915–1376	2.0000–2.1100	97
Schleifer, Naoumidis, and Nickel	37	1983	1129–1370	2.0050–2.0250	43
Ugajin	38	1983	1273–1473	2.0008–2.0954	18
Une and Oguma	39	1983	1273–1773	2.0000–2.0690	21

FIGURE 1

The entire T-x-RT ln ($p^*_{O_2}$) data base for $\langle UO_{2\pm x}\rangle$.

FIGURE 2

The ln($p^*_{O_2}$) dependence as a function of ln(x) for $\langle UO_{2+x}\rangle$ and of the logarithmic terms for several solid-solution models, eqs. (10-14), for a typical $\langle UO_{2+x}\rangle$ data set. Coincidence with the theoretical slope of 2 indicates the proper solution models.

FIGURE 3

All of the T-x-ln($p^*_{O_2}$) for $\langle UO_{2+x}\rangle$ data transformed to 1500 K via eqs. (20) and (25), with abcissa values determined from eqs. (21) and (26). The values of x appear at the top of the figure. The behavior predicted by the present representations is indicated, with the $[UO_2]$-$[U_3O_7]$ system giving a slope of 2 and the $[UO_2]$-$[U_2O_{4.5}]$ system a slope of 4. The prediction of Blackburn's model, his eq. (17a),[48] is also indicated. Analyzed data: ◇, AERE-Harwell, refs. 5, 8, 10, 14, 18, 24; + all others. Rejected data: □, ref. 12; Δ, ref. 20; ∇, ref. 31; 0, ref. 32.

FIGURE 4

Several representative T-x-ln($p^*_{O_2}$) data sets plotted as ln($p^*_{O_2}$) vs abcissa values determined from eqs. (21) and (26). The values of x appear at the top of the figure. The boundary, eq. (28), between the two hyperstoichiometric systems is indicated, and is consistent with the observed change in slope for the raw data.

FIGURE 5

All of the T-x-ln($p^*_{O_2}$) data for $\langle UO_{2-x}\rangle$ transformed to 2400 K, with the abscissa values determined from the ln term in eq. (43a). The values of x are shown at the bottom of the figure. The prediction of eq. (43a) is shown, with a slope of -3, as is the prediction of Blackburn's model, his eq. (11).[48] Data: 0, ref. 15; □, refs. 18, 23, 24; Δ, ref. 19; +, ref. 20; ◇, ref. 22; ∇, ref. 25; x, ref. 35.

FIGURE 6

The predicted behavior for the $\langle UO_{2\pm x}\rangle$ system plotted along with the raw data base from fig. 1. The high-temperature boundaries for $\langle UO_{2\pm x}\rangle$ were calculated from the two-phase equilibria involving $\langle UO_{2\pm x}\rangle$ and the U-O liquid phase, while the dotted line at ~-250 kJ/mol is from eq. (28), the boundary for the two $\langle UO_{2+x}\rangle$ representations.

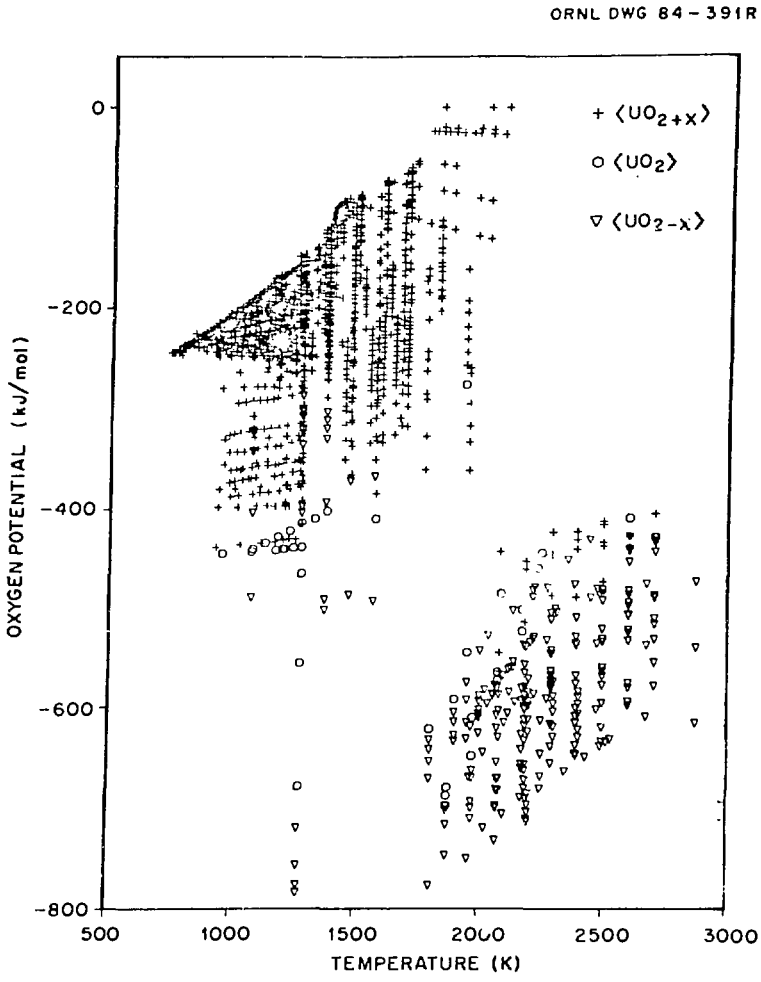

FIGURE 1

The entire T-x-RT ln ($p^*_{O_2}$) data base for $\langle UO_{2\pm x}\rangle$.

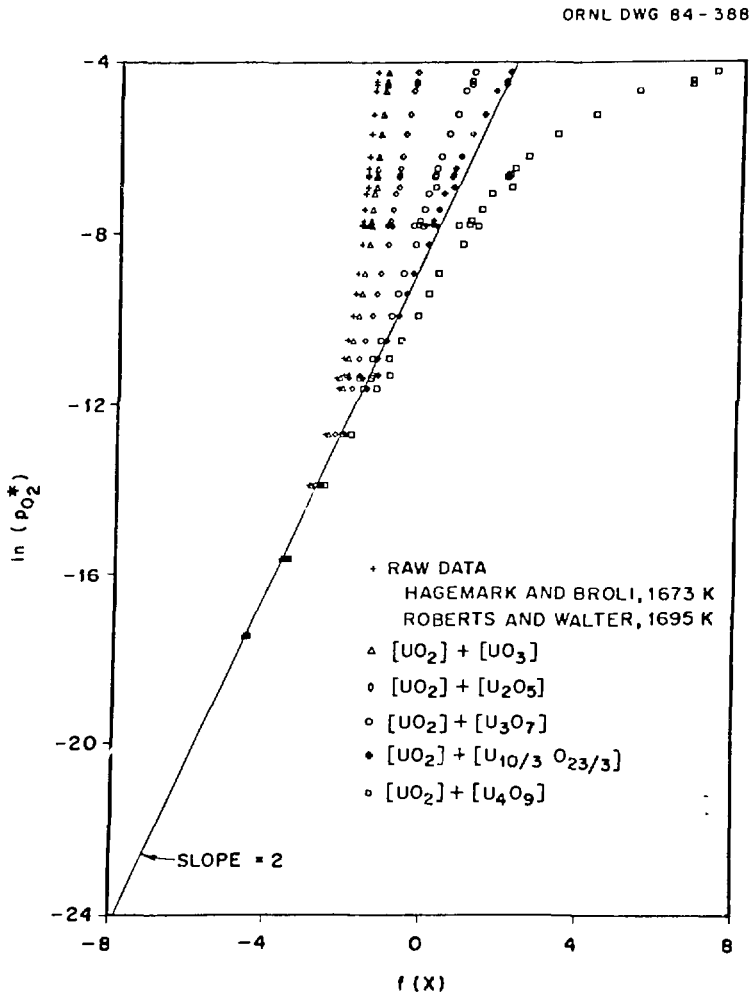

FIGURE 2

The $\ln(p_{O_2}^*)$ dependence as a function of ln(x) for $\langle UO_{2+x} \rangle$ and of the logarithmic terms for several solid-solution models, eqs. (10-14), for a typical $\langle UO_{2+x} \rangle$ data set. Coincidence with the theoretical slope of 2 indicates the proper solution models.

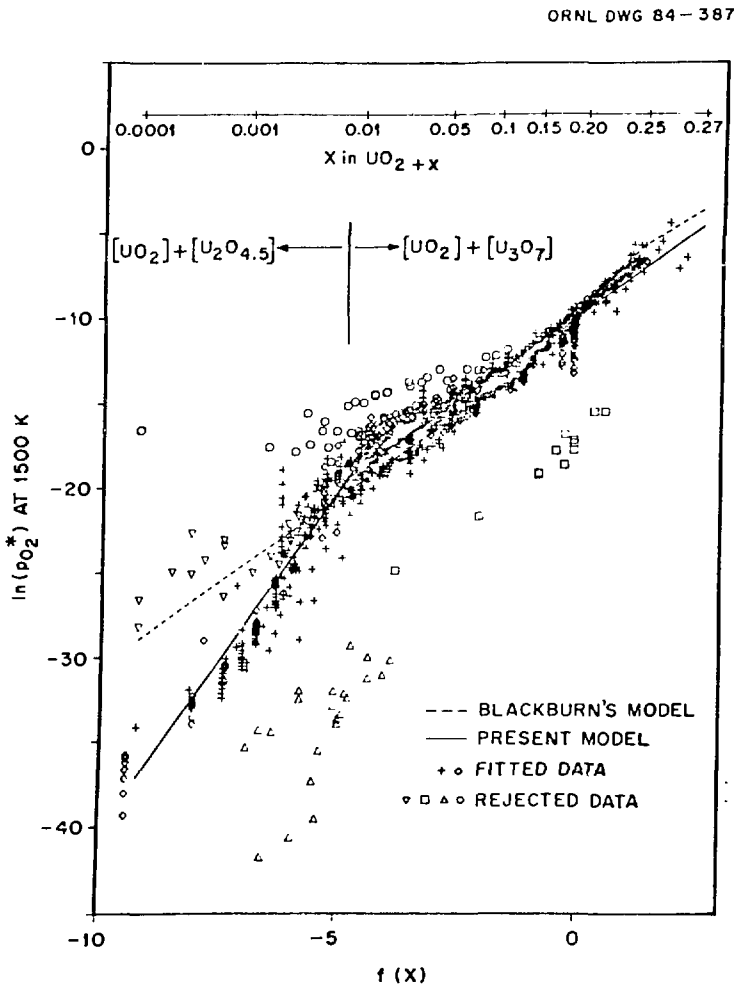

FIGURE 3

All of the T-x-$\ln(p^*_{O_2})$ for $\langle UO_{2+x} \rangle$ data transformed to 1500 K via eqs. (20) and (25), with abcissa values determined from eqs. (21) and (26). The values of x appear at the top of the figure. The behavior predicted by the present representations is indicated, with the $[UO_2]$-$[U_3O_7]$ system giving a slope of 2 and the $[UO_2]$-$[U_2O_{4.5}]$ system a slope of 4. The prediction of Blackburn's model, his eq. (17a),[48] is also indicated. Analyzed data: ◇, AERE-Harwell, refs. 5, 8, 10, 14, 18, 24; + all others. Rejected data: □, ref. 12; Δ, ref. 20; ∇, ref. 31; 0, ref. 32.

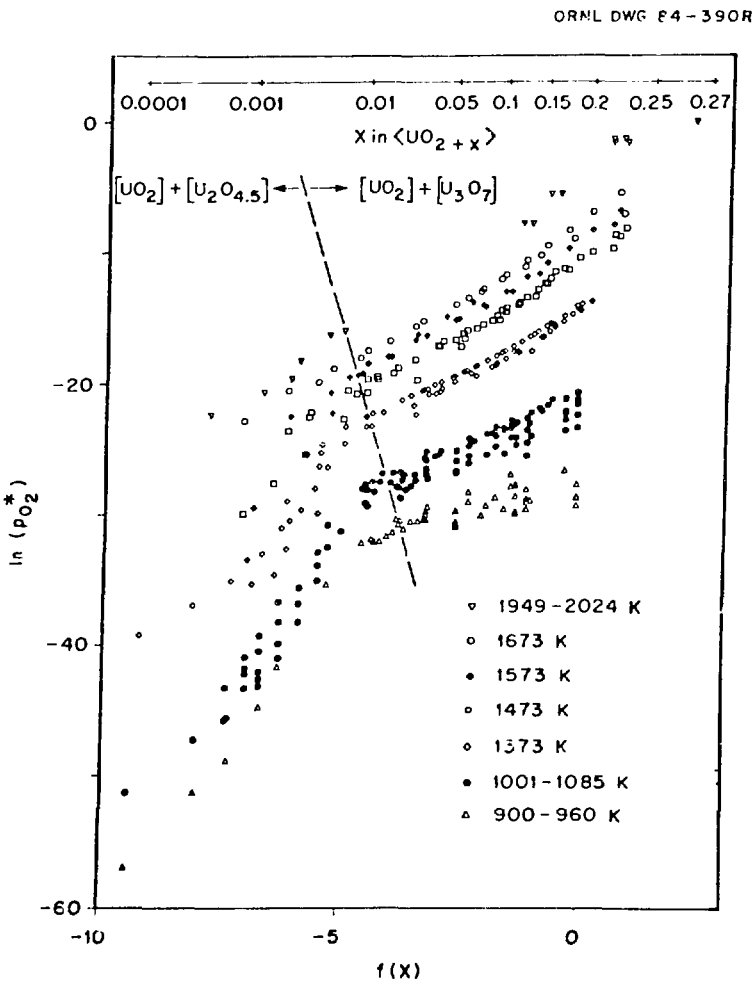

FIGURE 4

Several representative T-x-ln($p^*_{O_2}$) data sets plotted as ln($p^*_{O_2}$) vs abcissa values determined from eqs. (21) and (26). The values of x appear at the top of the figure. The boundary, eq. (28), between the two hyperstoichiometric systems is indicated, and is consistent with the observed change in slope for the raw data.

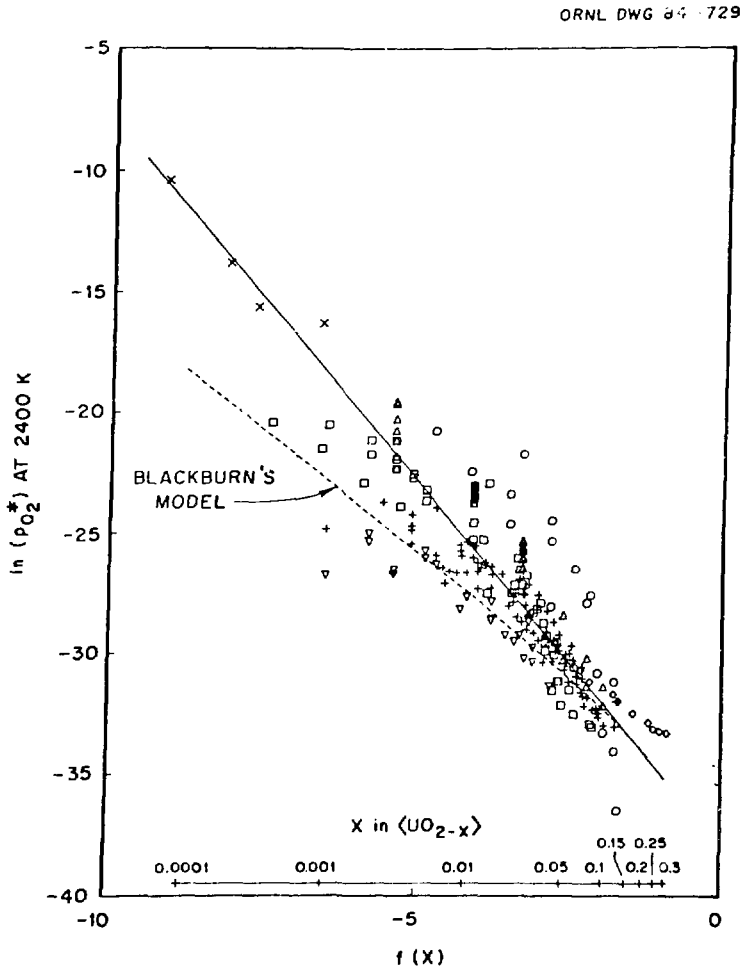

FIGURE 5

All of the T-x-ln($p^*_{O_2}$) data for $\langle UO_{2-x} \rangle$ transformed to 2400 K, with the abscissa values determined from the ln term in eq. (43a). The values of x are shown at the bottom of the figure. The prediction of eq. (43a) is shown, with a slope of -3, as is the prediction of Blackburn's model, his eq. (11).[48] Data: O, ref. 15; □, refs. 18, 23, 24; Δ, ref. 19; +, ref. 20; ◇, ref. 22; ▽, ref. 25; x, ref. 35.

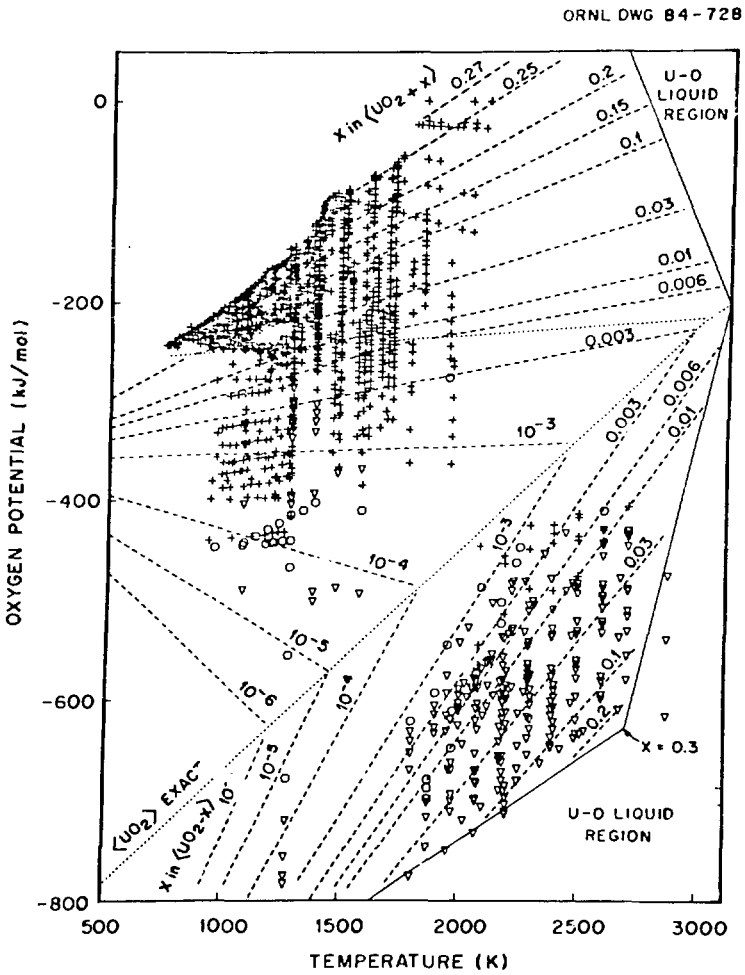

FIGURE 6

The predicted behavior for the $\langle UO_{2\pm x} \rangle$ system plotted along with the raw data base from fig. 1. The high-temperature boundaries for $\langle UO_{2\pm x} \rangle$ were calculated from the two-phase equilibria involving $\langle UO_{2\pm x} \rangle$ and the U-O liquid phase, while the dotted line at ~-250 kJ/mol is from eq. (28), the boundary for the two $\langle UO_{2+x} \rangle$ representations.